Manuscript Details

Manuscript number	FINEL_2017_791
Title	Numerical verification of an efficient coupled SAFE-3D FE analysis for guided wave ultrasound excitation
Article type	Research Paper

Abstract

Numerical verification of a method to simulate piezoelectric transducers exciting infinite elastic waveguides is presented. The method, referred to as SAFE-3D, combines a 3D finite element (FE) model of a transducer with a 2D semi-analytical finite element (SAFE) model of the waveguide. An interpolation procedure is employed to transfer forces and displacements between the SAFE and 3D FE models, and therefore nodes at the interface between the two models are not required to be coincident. An Abaqus/Explicit analysis, employing a thermal equivalent piezoelectric model and absorbing boundary conditions to prevent end reflections, is used to verify the accuracy of the SAFE-3D model. A piezoelectric transducer attached to the web of a rail and driven with frequency content which excites a mode cut-off is considered. A driving signal which does not contain cut-off frequencies is used for comparison. Time domain displacement results computed using Abaqus/Explicit and SAFE-3D are compared directly. Several methods to alleviate the numerical difficulties encountered by the SAFE-3D method, when transforming frequency domain displacements to the time domain, close to cut-off frequencies are evaluated. It is shown that post-processing methods have a similar effect to adding damping, but are less numerically expensive if iterative tuning of parameters is required. A SAFE-based method to extract modal amplitudes from Abaqus/Explicit time domain results is used to evaluate the accuracy of SAFE-3D in the frequency domain. Good agreement between the SAFE-3D method and results computed using Abaqus/Explicit is achieved, despite the Abaqus/Explicit and SAFE-3D models predicting slightly different cut-off frequencies.

Keywords	Semi-analytical finite element (SAFE); Piezoelectric transducer model; Cut-off frequency; Modal amplitude; Abaqus/Explicit; Rail

Corresponding Author	Craig Long
Order of Authors	Craig Long, Philip Loveday, Dineo Ramatlo, Eshwar Andhavarapu

Suggested reviewers	Fabien Treyssede, Ray Kirby, ivan bartoli, Prabhu Rajagopal

Submission Files Included in this PDF

File Name [File Type]

Long_etal_2008_FINEL_highlights.pdf [Highlights]

Long_etal_2008_FINEL_abstract.pdf [Abstract]

Long_etal_2008_FINEL.pdf [Manuscript File]

To view all the submission files, including those not included in the PDF, click on the manuscript title on your EVISE Homepage, then click 'Download zip file'.

Highlights

- Proposed SAFE-3D method, combining a 3D FE model of a piezoelectric transducer with a 2D SAFE model of a waveguide, without requiring coincident interface nodes.
- Numerical verification of the method by comparison with an Abaqus/Explicit analysis of a transducer attached to a rail web
- Time domain comparison including evaluation of methods to deal with resonant-like behaviour at cut-off frequencies
- Frequency domain comparison with modal amplitudes extracted from Abaqus/Explicit displacement results

Abstract

Numerical verification of a method to simulate piezoelectric transducers exciting infinite elastic waveguides is presented. The method, referred to as SAFE-3D, combines a 3D finite element (FE) model of a transducer with a 2D semi-analytical finite element (SAFE) model of the waveguide. An interpolation procedure is employed to transfer forces and displacements between the SAFE and 3D FE models, and therefore nodes at the interface between the two models are not required to be coincident. An Abaqus/Explicit analysis, employing a thermal equivalent piezoelectric model and absorbing boundary conditions to prevent end reflections, is used to verify the accuracy of the SAFE-3D model. A piezoelectric transducer attached to the web of a rail and driven with frequency content which excites a mode cut-off is considered. A driving signal which does not contain cut-off frequencies is used for comparison. Time domain displacement results computed using Abaqus/Explicit and SAFE-3D are compared directly. Several methods to alleviate the numerical difficulties encountered by the SAFE-3D method, when transforming frequency domain displacements to the time domain, close to cut-off frequencies are evaluated. It is shown that post-processing methods have a similar effect to adding damping, but are less numerically expensive if iterative tuning of parameters is required. A SAFE-based method to extract modal amplitudes from Abaqus/Explicit time domain results is used to evaluate the accuracy of SAFE-3D in the frequency domain. Good agreement between the SAFE-3D method and results computed using Abaqus/Explicit is achieved, despite the Abaqus/Explicit and SAFE-3D models predicting slightly different cut-off frequencies.

Numerical verification of an efficient coupled SAFE-3D FE analysis for guided wave ultrasound excitation

C.S. Long[a,*], P.W. Loveday[a], D.A Ramatlo[a], E.V. Andhavarapu[a]

[a] *CSIR Material Science and Manufacturing, P.O. Box 395, Pretoria, South Africa, 0001*

Abstract

Numerical verification of a method to simulate piezoelectric transducers exciting infinite elastic waveguides is presented. The method, referred to as SAFE-3D, combines a 3D finite element (FE) model of a transducer with a 2D semi-analytical finite element (SAFE) model of the waveguide. An interpolation procedure is employed to transfer forces and displacements between the SAFE and 3D FE models, and therefore nodes at the interface between the two models are not required to be coincident. An Abaqus/Explicit analysis, employing a thermal equivalent piezoelectric model and absorbing boundary conditions to prevent end reflections, is used to verify the accuracy of the SAFE-3D model. A piezoelectric transducer attached to the web of a rail and driven with frequency content which excites a mode cut-off is considered. A driving signal which does not contain cut-off frequencies is used for comparison. Time domain displacement results computed using Abaqus/Explicit and SAFE-3D are compared directly. Several methods to alleviate the numerical difficulties encountered by the SAFE-3D method, when transforming frequency domain displacements to the time domain, close to cut-off frequencies are evaluated. It is shown that post-processing methods have a similar effect to adding damping, but are less numerically expensive if iterative tuning of parameters is required. A SAFE-based method to extract modal amplitudes from Abaqus/Explicit time domain results is used to evaluate the accuracy of SAFE-3D in the frequency domain. Good agreement between the SAFE-3D method and results computed using Abaqus/Explicit is achieved, despite the Abaqus/Explicit and SAFE-3D models predicting slightly different cut-off frequencies.

*Corresponding author

Email address: clong@csir.co.za (C.S. Long)

Keywords: Semi-analytical finite element (SAFE), Piezoelectric transducer model, Cut-off frequency, Modal amplitude, Abaqus/Explicit, Rail

1. Introduction

Guided wave ultrasound (GWU) is well suited for inspection and monitoring applications of elongated structures such as plates, rods, pipes and rails [1]. By controlling which propagating modes are excited, and with knowledge of the propagation characteristics, systems can be design so that propagating energy can be distributed across the entire cross-section of the waveguide or concentrated in specific locations, or in geometrical features, depending on what damage is being sought. Guided waves can propagate long distance, especially when compared to conventional ultrasonic inspection (up to kilometers in some cases [2]). Furthermore, GWU is known to propagate in structures that are covered, submerged or buried reducing preparation efforts and cost. These properties make GWU very attractive for monitoring and inspection applications since long distance inspections can be carried out from a single stationary source.

In order to design a GWU-based non-destructive evaluation (NDE) system, it is necessary to understand how guided waves are excited, how they propagate (dispersion, attenuation, etc.), how they interact with discontinuities and damage (scattering) and finally how they are sensed (transduction). A conventional time-domain finite element analysis can be carried out to analyse the excitation, propagation, scattering and sensing. However, this type of analysis is generally very numerically expensive (if it is possible at all) especially at higher frequencies and over significant propagation distance, due to the fine spacial and temporal discretisation required. Furthermore, since the analysis is carried out in the time domain, modal information is not obtained directly and has to be extracted in some way. Due to these drawbacks, the semi-analytical finite element (SAFE) method [3, 4, 5] has become a popular analysis and design tool in the GWU community. The SAFE method naturally computes results based on their modal contributions and responses at significant distances can be estimated efficiently since the propagation direction (in which the structure is elongated) is treated analytically.

The focus of this paper is on the analysis of guided wave excitation. An efficient implementation of a method previously proposed by one of the

authors [6, 7] is presented, which allows several design iterations to be computed without having to solve the SAFE eigenvalue problem multiple times, and does not require transducer nodes to be coincident with the waveguide nodes. We also consider the performance of this method when exciting the waveguide at frequencies where modes cut-off on the frequency axis. These frequencies have previously been avoided [8].

Previous authors have considered the analysis of guided wave excitation. Willberg *et al.* [1] present an overview of relevant work, including a brief discussion of adhesive material, which we neglect in this study (but which could be included as a thin soft layer of elements between the transducer and the waveguide).

Lowe *et al.* [9] and Fateri *et al.* [10] consider an aluminium rod with a large (relative to the waveguide) transducer attached. They demonstrate the importance of including the transducer in the numerical model (as opposed to simply modelling the transducer as a distributed force). Reflections and mode conversion from a coupled piezoelectric transducer are considered. A full 3D Abaqus model of the waveguide and transducer is used for comparison with a single point excitation. At the excitation frequency considered in their work, there are only three possible propagating modes, L(0,1), T(0,1) and F(1,1), and the torsional mode is neglected. The comparison was performed in the time domain with modes separated based on Time of Arrival (ToA).

Kalkowski *et al.* [11] propose a technique based on the SAFE method for modelling waveguides with piezoelectric transducers attached. A piezoelectric SAFE element is presented and discrete piezoelectric elements are incorporated by computing scattering matrices at locations where geometry changes discretely. The proposed method is well suited to prismatic transducers (with regular shape in the propagation direction) such as simple rectangular patch and sandwich transducers, but may present difficulties when transducers have complex shape. Their proposed method is verified numerically using a simple beam model and validated experimentally with a short beam with anechoic terminations. The paper also presents a summary of some other relevant works.

Jezzine *et al.* [12] consider the case of a transducer fixed to a free end of a waveguide (i.e. on the arbitrary cross-section) using techniques similar to those employed for scattering from free ends and discontinuities [13]. They present comparison with analytical and previously published experimental results.

One of the authors of the current work previously proposed a method to

couple a SAFE model of the waveguide with a full 3D model of a piezoelectric transducer [6, 7]. The method involves computing the effective stiffness of the infinite waveguide, and then solving the transducer dynamics with the appropriate boundary condition, and then finally using the reaction forces from this analysis to compute the forced response of the waveguide. This method is generalised in this current work, so that the interface nodes between the SAFE and 3D meshes are not required to be coincident. This is accomplished by using a simple interpolation strategy. Furthermore, the resonance-like behaviour encountered when exciting a mode of propagation close to its cut-off frequency is studied and addressed. The procedure is compared with results from a time domain solution computed using the commercial finite element package Abaqus/Explicit.

2. Problem Formulation and Implementation

The presentation in this section will focus on the coupling of the 3D transducer FE model and the 2D waveguide SAFE model. More detail regarding the conventional SAFE formulation can be found in for example [3, 4, 5].

For the presentation, we will explicitly differentiate between displacements computed in the physical 3D domain and transformed displacements in the SAFE domain which are introduced in Section 2.2. Displacements in the 3D FE domain (which are assumed to be harmonic) are written as:

$$u_x(x, y, z, t) = u_x(x, y, z)e^{j\omega t} \tag{1}$$

$$u_y(x, y, z, t) = u_y(x, y, z)e^{j\omega t} \tag{2}$$

$$u_z(x, y, z, t) = u_z(x, y, z)e^{j\omega t} \tag{3}$$

where x, y and z are the global Cartesian coordinates, u_x, u_y and u_z are displacements in the x, y and z directions, respectively and ω is the angular frequency in time t, and j is the imaginary unit.

2.1. Piezoelectric finite element formulation

Piezoelectric transducers are often used to excite guided waves due to their ability to drive high frequencies. The formulation of conventional 3D finite elements is well know and will therefore not be presented here. Instead, only salient aspects of the piezoelectric implementation are presented. The

standard piezoelectric finite element implementation is employed, as originally proposed by Allik *et al.* [14].

The coupled constitutive piezoelectric relations can be written as:

$$\begin{aligned} \boldsymbol{\sigma}_u &= \boldsymbol{c}_E \boldsymbol{\epsilon}_u - \boldsymbol{e}^T \boldsymbol{\epsilon}_\phi, \\ \boldsymbol{\sigma}_\phi &= \boldsymbol{e} \boldsymbol{\epsilon}_u + \boldsymbol{p}_S \boldsymbol{\epsilon}_\phi, \end{aligned} \tag{4}$$

where $\boldsymbol{\sigma}_u$ represents the mechanical stress tensor while $\boldsymbol{\sigma}_\phi$ is the electric flux density, which is the electrical equivalent of stress. The strain is given by $\boldsymbol{\epsilon}_u$ while the electrical equivalent of strain is the electrical field $\boldsymbol{\epsilon}_\phi$ which is computed as the negative of the potential spacial gradient. The third order piezoelectric coupling tensor relating displacements u and potentials ϕ is denoted $\boldsymbol{e}$. The mechanical elasticity and dielectric constitutive matrices are represented by $\boldsymbol{c}_E$ and $\boldsymbol{p}_S$ respectively.

The harmonic response is computed by solving the linear system of equations which results from the finite element formulation, written as:

$$\begin{bmatrix} \boldsymbol{D}_t & \boldsymbol{K}_{u\phi} \\ \boldsymbol{K}_{u\phi}^T & \boldsymbol{K}_{\phi\phi} \end{bmatrix} \begin{Bmatrix} \boldsymbol{U} \\ \boldsymbol{\Phi} \end{Bmatrix} = \begin{Bmatrix} \boldsymbol{F} \\ \boldsymbol{Q} \end{Bmatrix} \tag{5}$$

where $\boldsymbol{U}$ and $\boldsymbol{\Phi}$ are the assembled nodal displacements and electrical potentials respectively and $\boldsymbol{F}$ and $\boldsymbol{Q}$ represent assembled forces and charges respectively. The stiffness matrix is made up of terms relating only to electrical properties $\boldsymbol{K}_{\phi\phi}$, those coupling electrical and mechanical properties $\boldsymbol{K}_{u\phi}$ and the frequency dependant dynamic stiffness of the transducer relating only to mechanical properties:

$$\boldsymbol{D}_t = \boldsymbol{K}_{uu} - \omega^2 \boldsymbol{M}. \tag{6}$$

These equations are partitioned into known and unknown degrees of freedom in order to solve unknown displacements and potentials as well as reaction forces and charges. If the model is of a transducer consisting of elastic and piezoelectric parts, electric potentials of elastic parts are simply prescribed to be zero.

2.2. SAFE formulation

The semi-analytical finite element (SAFE) formulation employed in this paper is based on that proposed by Gavrić [3]. This formulation is convenient since it results in symmetric stiffness matrices, eliminating the need for

solving both left and right eigenvalue problems [4, 15]. However, since only free vibrations were considered in [3], some detail needs to be added for the forced response problem. A one-dimensional waveguide with arbitrary cross-section in the $x-y$ plane and with wave propagation in the $z-$direction, is considered. The displacements are assumed to take the form:

$$u_x(x,y,z,t) = u_x(x,y)e^{-j(\kappa z-\omega t)} = \widehat{u_x}\,(x,y)e^{-j(\kappa z-\omega t)} \tag{7}$$

$$u_y(x,y,z,t) = u_y(x,y)e^{-j(\kappa z-\omega t)} = \widehat{u_y}\,(x,y)e^{-j(\kappa z-\omega t)} \tag{8}$$

$$u_z(x,y,z,t) = u_z(x,y)e^{-j(\kappa z-\omega t)} = j\ \widehat{u_z}\,(x,y)e^{-j(\kappa z-\omega t)}, \tag{9}$$

where $je^{-j(\kappa z-\omega t)} = e^{-j(\kappa z-\omega t-\pi/2)}$. These displacement equations can be written in vector form as

$$\boldsymbol{u}(x,y)e^{-j(\kappa z-\omega t)} = \boldsymbol{T}\,\widehat{\boldsymbol{u}}\,(x,y)e^{-j(\kappa z-\omega t)} \tag{10}$$

where displacements in the physical coordinate system (i.e. the coordinate system of the conventional 3D finite elements) are denoted $\boldsymbol{u}$. The transformed (SAFE) displacements, which presuppose a 90° phase shift between in-plane and out of plane displacements are denoted $\widehat{\boldsymbol{u}}$. A transformation matrix $\boldsymbol{T}$ which converts the SAFE displacements to physical displacements has been introduced, similar to that introduced by Damljanović *et al.* [5], and is defined as

$$\boldsymbol{T} = \begin{bmatrix} 1 & 0 & 0 \\ 0 & 1 & 0 \\ 0 & 0 & j \end{bmatrix}. \tag{11}$$

The transformation matrix has the following properties

$$\boldsymbol{T}\boldsymbol{T}^{*T} = \boldsymbol{T}^{*T}\boldsymbol{T} = \boldsymbol{I}, \tag{12}$$

where $(\cdot)^{*T}$ denotes the complex conjugate transpose, and the reverse of the transformation in (10) can be shown to be

$$\widehat{\boldsymbol{u}} = \boldsymbol{T}^{*T}\boldsymbol{u}. \tag{13}$$

The same transformation can be employed to convert generalised forces from physical forces in the global coordinate system, to the transformed SAFE forces. Although similar, the transformation matrix in (11) is the complex conjugate of that defined by Damljanović *et al.* [5, 16].

The variational formulation for the linear-elastic, small strain elastodynamics problem in the frequency domain is presented by Treyssède *et al.* [15] as:

$$\int_\Omega \delta\boldsymbol{\epsilon}^T\boldsymbol{\sigma}\mathrm{d}\Omega - \omega^2\int_\Omega \rho\delta\boldsymbol{u}^T\boldsymbol{u}\mathrm{d}\Omega = \int_\Omega \delta\boldsymbol{u}^T\boldsymbol{f}\mathrm{d}\Omega + \int_{\partial\Omega}\delta\boldsymbol{u}^T\boldsymbol{t}\mathrm{d}\partial\Omega \tag{14}$$

where, similar to Treysséde [17] (but with displacements defined here being conjugate to the implementation presented by [17]):

$$\boldsymbol{u} = \boldsymbol{u}(x,y)e^{-j(\kappa z-\omega t)}, \quad \text{and } \delta\boldsymbol{u} = \delta\boldsymbol{u}(x,y)e^{j(\kappa z-\omega t)}. \tag{15}$$

After substitution of the interpolated displacement fields into (14), and employing the definition of linear strain and the constitutive relations between stress and strain, the following system of equations result [6, 7]

$$\left[-\omega^2\boldsymbol{M} + \kappa^2\boldsymbol{K}_2 + \kappa\boldsymbol{K}_1 + \boldsymbol{K}_0\right]\widehat{\boldsymbol{U}} = \widehat{\boldsymbol{F}}\ . \tag{16}$$

The vectors $\widehat{\boldsymbol{U}}\ (\omega,\kappa)$ and $\widehat{\boldsymbol{F}}\ (\omega,\kappa)$ represent the transformed nodal displacements and forces respectively, so for example $\widehat{\boldsymbol{F}} = \boldsymbol{T}^{*T}\boldsymbol{F}$, where $\boldsymbol{F}$ are the nodal forces in the physical coordinates, and in this case the transformation matrix is a diagonal matrix similar to that introduced in (11) with ones on the diagonal except every third term which has a j, but is of size $3N \times 3N$ where N is the number of SAFE nodes. Written explicitly:

$$\widehat{\boldsymbol{F}} = \begin{bmatrix} 1 & 0 & 0 & \dots \\ 0 & 1 & 0 & \dots \\ 0 & 0 & -j & \dots \\ \vdots & \vdots & \vdots & \ddots \end{bmatrix} \begin{Bmatrix} f_{1x} \\ f_{1y} \\ f_{1z} \\ \vdots \\ f_{Nz} \end{Bmatrix} = \begin{Bmatrix} f_{1x} \\ f_{1y} \\ -jf_{1z} \\ \vdots \\ -jf_{Nz} \end{Bmatrix} \tag{17}$$

Individual mass and stiffness matrices in (16), which are all symmetrical in

this case, are defined as

$$\boldsymbol{K}_0 = \int_\Omega \left[\boldsymbol{B}_0^{*T} \boldsymbol{C} \boldsymbol{B}_0\right] \mathrm{d}\Omega \tag{18}$$

$$\boldsymbol{K}_1 = \int_\Omega \left[\boldsymbol{B}_0^{*T} \boldsymbol{C} \boldsymbol{B}_1 + \boldsymbol{B}_1^{*T} \boldsymbol{C} \boldsymbol{B}_0\right] \mathrm{d}\Omega \tag{19}$$

$$\boldsymbol{K}_2 = \int_\Omega \left[\boldsymbol{B}_1^{*T} \boldsymbol{C} \boldsymbol{B}_1\right] \mathrm{d}\Omega \tag{20}$$

$$\boldsymbol{M} = \int_\Omega \left[\boldsymbol{N}^T \rho \boldsymbol{N}\right] \mathrm{d}\Omega \tag{21}$$

where $\boldsymbol{B}_0$ and $\boldsymbol{B}_1$ are strain-displacement operators which have been separated into terms containing and those not containing the wavenumber κ, respectively. $\boldsymbol{C}$ is the constitutive matrix relating stress and strain $\boldsymbol{\sigma} = \boldsymbol{C}\boldsymbol{\epsilon}$, $\boldsymbol{N}$ is a matrix containing shape functions and ρ is the material mass density. The mass and stiffness matrices are not explicitly shown as being formulated in the SAFE space as, for example $\widehat{\boldsymbol{K}}_0$. This is implied since both the displacements and forces are in the SAFE space.

2.3. Solution of the Free and Forced Vibration Problems

The forced response will be used to estimate the frequency dependant stiffness of the waveguide for each degree of freedom of the 3D transducer model that is in contact with the waveguide. The forced response problem was considered by [4, 5, 15]. Equation (16) is cast in linear form as

$$\left[\boldsymbol{\mathcal{A}} - \kappa \boldsymbol{\mathcal{B}}\right] \widehat{\boldsymbol{\mathcal{U}}} = \widehat{\boldsymbol{\mathcal{F}}} \tag{22}$$

where:

$$\boldsymbol{\mathcal{A}} = \begin{bmatrix} \boldsymbol{K}_0 - \omega^2 \boldsymbol{M} & \boldsymbol{0} \\ \boldsymbol{0} & -\boldsymbol{K}_2 \end{bmatrix}, \boldsymbol{\mathcal{B}} = \begin{bmatrix} -\boldsymbol{K}_1 & -\boldsymbol{K}_2 \\ -\boldsymbol{K}_2 & \boldsymbol{0} \end{bmatrix} \tag{23}$$

and

$$\widehat{\boldsymbol{\mathcal{U}}}\left(\omega, \kappa\right) = \begin{Bmatrix} \widehat{\boldsymbol{U}} \\ \kappa\, \widehat{\boldsymbol{U}} \end{Bmatrix}, \ \widehat{\boldsymbol{\mathcal{F}}}\left(\omega, \kappa\right) = \begin{Bmatrix} \widehat{\boldsymbol{F}} \\ \boldsymbol{0} \end{Bmatrix} \tag{24}$$

The homogeneous form of (22) can be used to compute a set of wavenumbers κ_i and associated mode shapes $\widehat{\boldsymbol{\psi}}_i$ at a fixed frequency ω from the eigen-

vectors

$$\widehat{\boldsymbol{\Psi}}_i = \left\{ \begin{array}{c} \widehat{\boldsymbol{\psi}}_i \\ \kappa\, \widehat{\boldsymbol{\psi}}_i \end{array} \right\}. \tag{25}$$

Treysséde *et al.* [15] then show how the solution of the forced response problem can be written as an expansion of the modes, and also how the inverse Fourier transform of the displacement solution can be computed using the Cauchy residue theorem to yield a response $\widehat{\boldsymbol{U}}$ in the transformed SAFE space-time domain, which in our case is given by:

$$\widehat{\boldsymbol{U}}\,(\omega, z) = j \sum_{r=1}^{3N} \widehat{\boldsymbol{\psi}}_r \, \frac{\widehat{\boldsymbol{\Psi}}_r^{\,T} \widehat{\boldsymbol{\mathcal{F}}}}{\widehat{\boldsymbol{\Psi}}_r^{\,T} \boldsymbol{\mathcal{B}}\, \widehat{\boldsymbol{\Psi}}_r} e^{-j\kappa_r z}, \tag{26}$$

where the summation is performed only over the positive real poles, negative imaginary poles, and complex poles with negative imaginary parts. During the calculations leading to (26) it is important to keep in mind the displacement definitions which were defined in (10), noting that our definition is the complex conjugate of that used by Hayashi *et al.* [4] and Treysséde *et al.* [15]. Furthermore, since our eigenvalue problem is symmetrical, it is not necessary to compute left and right eigenvalues, simplifying the orthogonality conditions used to arrive at (26).

The displacement response is a superposition of the response of each mode, and can be written in terms of the modal amplitudes α_r as:

$$\widehat{\boldsymbol{U}}\,(z, \omega) = \sum_{r=1}^{3N} \alpha_r e^{-j\kappa_r z}\, \widehat{\boldsymbol{\psi}}_r, \quad \text{where } \alpha_r = j \frac{\widehat{\boldsymbol{\Psi}}_r^{\,T} \widehat{\boldsymbol{\mathcal{F}}}}{\widehat{\boldsymbol{\Psi}}_r^{\,T} \boldsymbol{\mathcal{B}}\, \widehat{\boldsymbol{\Psi}}_r}. \tag{27}$$

Storing the modal amplitudes has the advantage that it is not necessary to re-calculate their values should the displacement be required at various distances z along the waveguide.

To convert these SAFE displacements back to physical displacements in the global coordinate system, the transformation

$$\boldsymbol{U}(z, \omega) = \boldsymbol{T}\, \widehat{\boldsymbol{U}}\,(z, \omega) \tag{28}$$

is again employed, where $\boldsymbol{T}$ is as previously defined.

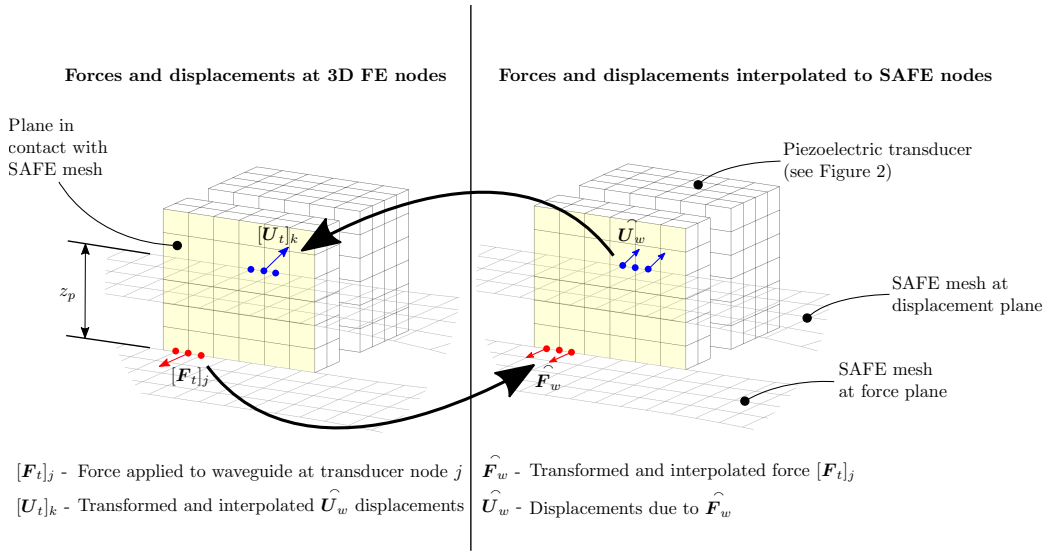

Figure 1: Mapping between 3D FE dofs and SAFE dofs.

Tresséde *et al.* [15] point out that the summation of modes should be carried out over forward propagating modes as determined from the sign of the energy velocity (or group velocity where applicable). They also briefly discuss the calculation of backward propagating modes. They further note that the modes can be truncated based on the size of the imaginary part of $(\kappa \cdot z)$. Finally, the response in space-time can be computed by taking the inverse temporal Fourier transform of $\boldsymbol{U}(z, \omega)$.

2.4. Coupling the SAFE and 3D models

The forced response solution presented in the previous section can be used to estimate the frequency-dependant dynamic stiffness that a transducer attached to a waveguide would experience. The dynamic stiffness matrix of the waveguide $\boldsymbol{D}_w$ relates a force applied at a specific transducer location $\boldsymbol{F}_t$ to a displacement at a different transducer location $\boldsymbol{U}_t$ as:

$$\boldsymbol{D}_w \boldsymbol{U}_t = \boldsymbol{F}_t \tag{29}$$

The receptance of the waveguide $\boldsymbol{R}_w = \boldsymbol{D}_w^{-1}$ can be computed row-by-row by applying a unit forces at each transducer degree of freedom, and computing the displacements at each of the transducer degrees of freedom in contact with the waveguide. We will not require here that the transducer

and the SAFE model nodes are coincident as in [6, 7]. Instead, appropriate element interpolation functions are used to interpolate between the two domains (SAFE and FE).

In order to treat the coupling between the SAFE and the 3D FE transducer model meshes, first the following sets (and associated number of dofs) are defined:

- N_w - Total number of waveguide (SAFE) dofs.
- N'_w - Limited number of waveguide dofs in contact with the 3D transducer.
- N_t - Total number of transducer (3D FE) dofs.
- N'_t - Limited number of transducer dofs in contact with the waveguide.

2.4.1. Step 1. Unit-force modal amplitudes

The first step in this process is to compute the unit-force modal amplitudes. In (27), $\boldsymbol{\alpha}$ is a vector corresponding to the modal amplitude of each mode as a result of the single applied force considered. To begin, we now compute an array $\bar{\boldsymbol{\alpha}}_k$, where

$$\bar{\alpha}_{r,k} = j \frac{\widehat{\boldsymbol{\Psi}}_r^T \widehat{\boldsymbol{\mathcal{F}}}_k}{\widehat{\boldsymbol{\Psi}}_r^T \boldsymbol{\mathcal{B}} \widehat{\boldsymbol{\Psi}}_r} \tag{30}$$

where $\widehat{\boldsymbol{\mathcal{F}}}_k$ is the force term due to applying a unit force $\bar{\boldsymbol{F}}_k$ in the global coordinate system to each of the N'_w degrees of freedom. The unit force is assembled into the $\boldsymbol{\mathcal{F}}_k$ vector and transformed using $\widehat{\boldsymbol{\mathcal{F}}}_k = \boldsymbol{T}^{*T} \boldsymbol{\mathcal{F}}_k$. This full $\bar{\boldsymbol{\alpha}}_k$ array will be used later to reconstruct a modal amplitude vector which is the cumulative sum of all the forces from the transducer using the superposition principle. The array of unit-force modal amplitudes and the associated array size is denoted $[\bar{\boldsymbol{\alpha}}]_{N_w, N'_w}$ where the subscript indicates the array size.

2.4.2. Step 2. Interpolation between meshes

Next, the array $[\boldsymbol{\mathcal{N}}]_{N'_t, N'_w}$ which maps the transducer degrees of freedom to the corresponding waveguide degrees of freedom is defined, making use

of the SAFE interpolation functions $\boldsymbol{N}$, evaluated at the transducer nodal locations for each of the N_t' transducer degrees of freedom.

Transducer forces can therefore be converted to waveguide forces using

$$\boldsymbol{F}_w = ([\boldsymbol{\mathcal{N}}]_{N_t',N_w'})^T \boldsymbol{F}_t, \tag{31}$$

whereas the waveguide displacements can be converted from the SAFE mesh to the 3D transducer mesh using

$$\boldsymbol{U}_t = [\boldsymbol{\mathcal{N}}]_{N_t',N_w'} \boldsymbol{U}_w. \tag{32}$$

Note that in both instances, the quantities are in physical coordinates, and it is therefore assumed that the waveguide displacements are computed using $\widehat{\boldsymbol{F}}_w = \boldsymbol{T}^{*T} \boldsymbol{F}_w$, and physical waveguide displacements are given by $\boldsymbol{U}_t = \boldsymbol{T}\, \widehat{\boldsymbol{U}}_w$. This mapping is illustrated in Figure 1.

2.4.3. Step 3. Assembly of the receptance and dynamic stiffness matrix

The third step in the process is to construct the receptance matrix $\boldsymbol{R}_w$ of size $(N_t' \times N_t')$ making use of the already computed $\bar{\boldsymbol{\alpha}}_k$ values. The waveguide displacements are computed using the distance along the propagation direction between the point where the transducer force is applied, and the point where the transducer displacement dof is computed. This distance is denoted z_p, see Figure 1.

The modal amplitudes $\bar{\boldsymbol{\alpha}}_k$ can be used to compute the response of all SAFE displacements due to the unit forces at each N_w' dofs using

$$\widehat{U}_{r,k} = \sum_{r=1}^{3N} \bar{\alpha}_{r,k} e^{-j\kappa_r z_p}\, \widehat{\boldsymbol{\psi}}_r, \tag{33}$$

where $\widehat{\boldsymbol{U}}_k$ is the same size as $\bar{\boldsymbol{\alpha}}_k$, i.e. $N_w \times N_w'$. From this array, the limited array of responses at waveguide displacements in contact with the transducer can be extracted, so that the size of $\widehat{\boldsymbol{U}}_k$ is reduced to $[\widehat{\boldsymbol{U}}_k]_{N_w',N_w'}$

These displacements due to unit forces at each waveguide dof are then summed to give the actual waveguide forces due to a unit transducer force as follows:

$$\widehat{\boldsymbol{U}}_w = [\widehat{\boldsymbol{U}}_k]_{N_w',N_w'} (\boldsymbol{\mathcal{N}}\, \widehat{\boldsymbol{F}}_t). \tag{34}$$

The waveguide displacements can be converted to transducer displacements in the physical coordinate system using the transformation matrix $\boldsymbol{T}$:

$$\boldsymbol{U}_t = \boldsymbol{T}([\boldsymbol{\mathcal{N}}_w]_{N_t',N_w'}\ \widehat{\boldsymbol{U}}_w). \tag{35}$$

This displacement is used to assemble the receptance matrix of the waveguide $\boldsymbol{R}_w$. $R_{w[i,j]}$ is the displacement ($U_{t[j]}$) at transducer dof j as a result of unit force applied at transducer dof i ($F_{t[i]}$). The dynamic stiffness matrix is then simply the inverse of $\boldsymbol{R}_w$:

$$[\boldsymbol{D}_w]_{N_t',N_t'} = (\boldsymbol{R}_w)^{-1}. \tag{36}$$

2.4.4. Step 4. Computation of transducer response and waveguide forces

The fourth step in the process is to use the computed dynamic stiffness matrix to compute transducer response. The waveguide dynamic stiffness matrix $\boldsymbol{D}_w$ can be added to the appropriate degrees of freedom of the transducer dynamic stiffness matrix (6) and then the forced response of the transducer as a result of prescribed voltage can be solved using (5). Using these computed transducer displacements $\boldsymbol{U}_t$, the forces that the waveguide experiences as a result of the interaction can be computed at the transducer nodal locations as

$$\boldsymbol{F}_t = \boldsymbol{D}_w\boldsymbol{U}_t. \tag{37}$$

2.4.5. Step 5. Waveguide response due to transducer dynamics

Finally, the previously computed modal amplitudes due to applied unit forces (30), can be scaled using the actual forces (37) at the transducer locations and propagated to a common waveguide $z-$plane (the $z-$plane at the contact point with the largest z is selected for this purpose) so that further propagation can be computed from a common location.

The modal amplitude at the front plane of the transducer, due to each of the transducer forces $F_{t[i]}$, is computed as:

$$\boldsymbol{\alpha}_{N_w,1} = \sum_{j=1}^{N_t'}([\bar{\boldsymbol{\alpha}}e^{-j\boldsymbol{\kappa}z_f}]_{N_w,N_w'})(\{\boldsymbol{\mathcal{N}}\ \widehat{\boldsymbol{F}}_{t\ j}\}_{N_w',1}), \tag{38}$$

where in this case z_f is the distance from the force $z-$plane to the plane at the front of the transducer. It should also be noted that the transducer forces once again need to be transformed to SAFE forces.

The response of an elastic waveguide at a distance from the front of the transducer can be computed using (27) and (28).

2.4.6. Implementation notes

In order to improve the numerical efficiency of the solution, especially if different attachment locations for the same transducer are going to be evaluated, or if different transducers are to be evaluated on the same waveguide [8], the following observations can be made:

- The symmetry properties of the receptance matrix $\boldsymbol{R}_w$ can be exploited in order to only consider forward propagation (i.e. only computing responses at nodes in the $z-$plane of each transducer node and those in forward $z-$planes). $\boldsymbol{R}_w$ is symmetric, except for the coupling terms between the $x-$ and $y-$directions and the $z-$direction, which is skew-symmetric.

- The wavenumbers and modes shapes of a particular waveguide as well as the modal amplitudes (38) associated with a transducer and transducer location can be stored at each frequency. Storing the SAFE data reduces solution times for different transducers (or transducer locations) on the same waveguide, while storing the modal amplitudes reduces solution times when computing time domain responses at different propagation distances for a specific transducer at a specific location.

3. Treatment of modes excited close to cut-off frequency

Exciting a guided wave mode at, or close to its cut-off frequency is known to result in resonant-like behaviour, analogous to exciting a mode of vibration in a finite structure at its resonant frequency. In the absence of damping the steady-state response at the cut-off frequency becomes unbounded. This behaviour causes numerical difficulties when converting frequency domain results to the time domain, as may be required when using the SAFE-3D analysis described here. The time domain result at cut-off is dominated by this resonant-like response at the cut-off frequency which manifests as a ringing which wraps-around in the time domain.

These difficulties are effectively controlled by introducing damping into the system [18, 19]. However, realistic values for damping are usually difficult

to estimate *a priori* and are usually iteratively determined through experimental comparison. This can be numerically quite expensive since for each damping value evaluated the SAFE eigenvalue problem needs to be re-solved.

Post-processing or filtering methods, which can be applied without having to resolve the SAFE eigenvalue problem, have also been proposed. Stoyko [20] proposed eliminating the wrap-around effect by adding a homogeneous solution consisting of the response of each mode at cut-off, and using this to enforce the initial displacement and velocity conditions, which are not necessarily satisfied using the inverse Fourier transform. This process is referred to in [20] as enforcing causality. An alternative post-processing method is to simply eliminate the large responses at cut-off by effectively filtering the contribution of the modes in the proximity of the cut-off frequency [21]. High phase velocities or low wavenumber thresholds can be used to identify modes at cut-off. Another method, which is not evaluated here, but which may be considered is to add a small imaginary part to the input frequency as proposed in Mukdadi *et al.* [22].

Post-processing methods and the inclusion of damping are evaluated in this study. Details of the methods evaluated are as follows:

- Causality was enforced as proposed by Stoyko [20]. Only modes which cut-off in the frequency range of interest were used to compute the homogeneous solution. The amplitude and phase of the cut-off modes were computed so as to best enforce the initial conditions (zero initial displacement and velocity at each dof) in a least-squares sense.

- The filtering method was implemented by simply setting modal amplitudes (38) to zero if the phase velocity associated with the modal amplitude was greater than twice the maximum group velocity in the frequency range of interest. This limit is depicted in Figure 4b, and although it may appear very aggressive it was found to be appropriate if relatively few frequency points are used.

- In order to damp the large response at cut-off, hysteretic damping is employed with complex bulk velocities as defined in [18, 19]. Bartoli *et al.* [19] showed that in the frequency range of interest here, longitudinal and shear bulk wave attenuation of κ_L=0.003 Np/wavelength and κ_T=0.043 Np/wavelength respectively are appropriate. Since these values are not always well know, the effects of over- and under-estimating

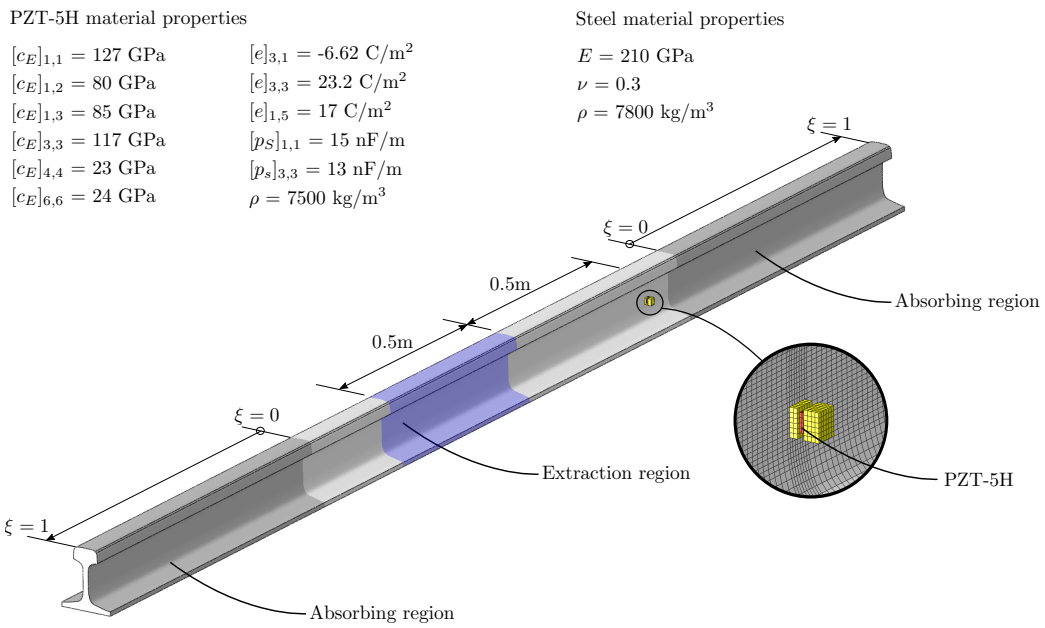

Figure 2: Abaqus/Explicit model of rail with piezoelectric transducer attached.

the damping are simulated by using damping constants 10 times greater and 10 times smaller than those proposed in [19].

4. Abaqus model and mode extraction

In this section, some details regarding the Abaqus/Explicit model used to verify the accuracy of the SAFE-3D results, are presented. Three topics are briefly treated, namely absorbing boundary conditions to prevent reflections from free ends of the 3D FE models, the thermal equivalent piezoelectric model employed in Abaqus/Explicit and finally the method used to perform mode extraction from the 3D FE time domain results.

Figure 2 illustrates the problem under consideration. A rectangular piezoelectric transducer is modelled, with common nodes on the interface plane between the transducer and the rail web, so as to avoid having to use contact models in the Abaqus/Explicit simulation. Coincident nodes are not required for the SAFE-3D method presented herein, as demonstrated in Figure 8b and by Ramatlo *et al.* [8].

4.1. Absorbing boundary conditions

In order to extract modes excited by the transducer in the time domain, relatively long displacement time traces are required. This is especially true when different modes travel at significantly different speeds or when exciting modes close to their cut-off frequency, due to the ringing-like behaviour observed. When considering relatively long simulation times in the time domain, complex mode coupling due to end reflections adds unwanted complexity. It is therefore advantageous to be able remove these end reflections in order to simulate an infinitely long rail.

The problem of eliminating end reflections has been studied by various authors. Two methods which can relatively easily be implmented using commercial codes were proposed by Rajagopal *et al.* [23] (Absorbing Layers using Increasing Damping (ALID)) and Pettit *et al.* [24] (stiffness reduction method). A hybrid method, combing stiffness reduction and increased damping, was found to work well in this instance for one-dimensional wave propagation.

In the absorbing region, a local coordinate, $0 < \xi \leq 1$ is introduced, with $\xi = 0$ at the start of the absorbing region and $\xi = 1$ at the free end of the waveguide as depicted in Figure 2. A damping factor ($0 \leq d \leq 1$) and a stiffness factor ($0 < s \leq 1$) are then defined as:

$$d(\xi) = \xi^p \tag{39}$$

$$s(\xi) = e^{-d(\xi)\cdot p} - \xi \cdot (e^{-p} - \epsilon) \tag{40}$$

where p is a penalty parameter and the second term in (40) ensures that the stiffness parameter ends with a small value ϵ. These functions are depicted graphically in Figure 3 for a penalty parameter of $p = 3$ which was used to generate the result in Section 5.

For each element in the absorbing region, the local coordinate of the element centroid is determined and the modified elastic modulus E^* and Rayleigh mass proportional damping constant α^* for the element is computed as

$$E^* = s \cdot E_0, \text{ and } \alpha^* = d \cdot \alpha_{\max}, \tag{41}$$

where E_0 is the elastic modulus of the waveguide material and $\alpha_{\max}$ is the maximum value of Rayleigh mass proportional damping, which is set to the centre circular frequency of the driving signal as suggested in [24].

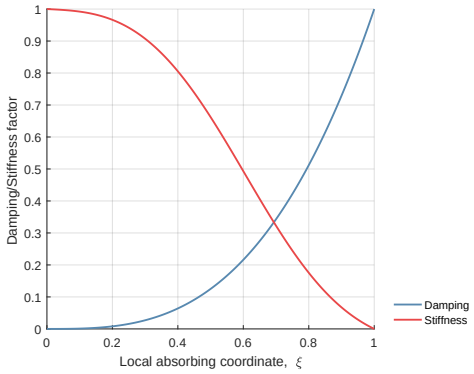

Figure 3: Stiffness factor s and damping factor d for local coordinate $0 \leq \xi \leq 1$ and penalty parameter $p = 3$.

4.2. Thermal equivalent piezoelectric model

Since Abaqus/Explicit does not include piezoelectric effects, a thermal equivalent piezoelectric model is used to simulate piezoelectric excitation. This is simply achieved by defining an orthotropic thermal coefficient of expansion for the piezoelectric materials in the model (with orthotropic elastic coefficients $\boldsymbol{c}_E$ as defined in (4)). The orthotropic thermal coefficients of expansion are extracted from the matrix $\boldsymbol{d}$ when the piezoelectric constitutive laws are written with stress and electric field as independent variables as in (42) instead of strain and electric field as in (4).

$$\begin{aligned} \boldsymbol{\epsilon}_u &= \boldsymbol{s}_E \boldsymbol{\sigma}_u + \boldsymbol{d}^T \boldsymbol{\epsilon}_\phi \\ \boldsymbol{\sigma}_\phi &= \boldsymbol{d} \boldsymbol{\sigma}_u + \boldsymbol{p}_T \boldsymbol{\epsilon}_\phi, \end{aligned} \tag{42}$$

where $\boldsymbol{s}_E = \boldsymbol{c}_E^{-1}$, $\boldsymbol{d} = \boldsymbol{e} \cdot \boldsymbol{s}_E$ and $\boldsymbol{p}_T = \boldsymbol{p}_S + \boldsymbol{d} \cdot \boldsymbol{c}_E \cdot \boldsymbol{d}^T$. The electric field due to the time-varying prescribed voltages is then simply simulated as a temperature, with all non-piezoelectric materials having zero coefficient of thermal expansion.

4.3. Mode extraction from time domain results

In order to compare numerical time-domain results with mode-based results in the frequency domain computed using the SAFE-3D analysis, a method to identify and quantify which modes are excited is required. This is not a trivial task due to the multi-modal and dispersive nature of guided wave propagation [25].

Zhao *et al.* [26] reviews some methods for mode identification and extraction. If modes are separated in time, a simple time gating approach could be employed. Otherwise, for mode extraction or identification a Short Time Fourier Transform (STFT) can be used as in [27, 28]. Alternatively, a 2D Fast Fourier Transform (FFT) can be used, as for example in Pavlakovic *et al.* [28], who present a method to excite a pure mode in the time domain and then employ a 2D FFT to analyse purity of the excited mode.

The method employed in this work decomposes extracted displacements into modal contributions using SAFE information, and has been successfully used to extract modes (and modal amplitudes) from experimental measurements [29, 30]. The displacement response at a specific degree of freedom in the SAFE mesh i at distance z can be written in the physical coordinate system as (see (27)):

$$U_i(z,\omega) = \sum_{r=1}^{3N} \psi_{ir}(\omega)\alpha_r(\omega)e^{-j\kappa_r(\omega)z}, \tag{43}$$

where $\psi_{ir}(\omega)$ is the displacement of degree of freedom i of mode shape r and $\kappa_r(\omega)$is the wavenumber of mode r. The mode shape and wavenumber are computed using a SAFE analysis. We wish to extract the magnitude of each propagating mode $\alpha_r(\omega)$ from numerical time responses $U_i(z,\omega)$.

For p time traces of Abaqus/Explicit nodes corresponding to SAFE nodes, this can be written in matrix form as

$$\bar{\boldsymbol{\Psi}}(\omega)\boldsymbol{\alpha}(\omega) = \boldsymbol{U}(\omega), \tag{44}$$

where, if the frequency dependence of ψ, α and U are implied,

$$\begin{bmatrix} \psi_{11}e^{-j\kappa_1 z_1} & \psi_{12}e^{-j\kappa_2 z_1} & \cdots & \psi_{1m}e^{-j\kappa_m z_1} \\ \vdots & \vdots & & \vdots \\ \psi_{p1}e^{-j\kappa_1 z_p} & \psi_{p2}e^{-j\kappa_2 z_p} & \cdots & \psi_{pm}e^{-j\kappa_m z_p} \end{bmatrix} \begin{Bmatrix} \alpha_1 \\ \vdots \\ \alpha_m \end{Bmatrix} = \begin{Bmatrix} U_1 \\ \vdots \\ U_p \end{Bmatrix}. \tag{45}$$

The mode shape matrix $\bar{\boldsymbol{\Psi}}$ is assembled from information from the SAFE model while vector $\boldsymbol{U}$ is assembled by performing a FFT on each of the extracted time domain Abaqus/Explicit displacement signals at various propagation distances z. In order to perform the FFT, the Abaqus/Explicit results need to be interpolated so that the time increment is the same for every time step. Matrix $\bar{\boldsymbol{\Psi}}$ has dimension $[p \times m]$, while $\boldsymbol{\alpha}$ is $[m \times 1]$ and $\boldsymbol{U}$ is $[p \times 1]$.

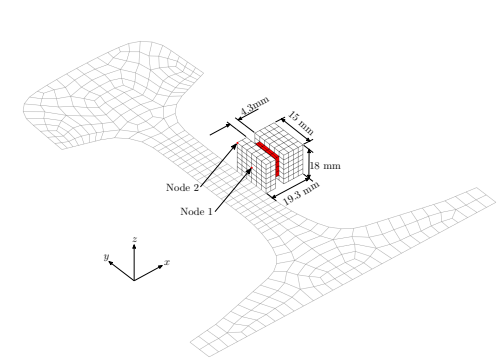

(a) SAFE mesh with transducer attached.

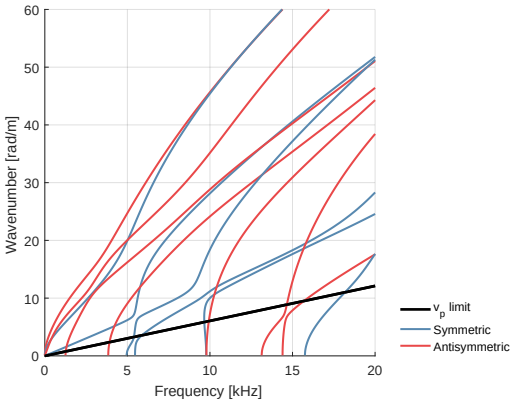

(b) Wavenumber-Frequency curves.

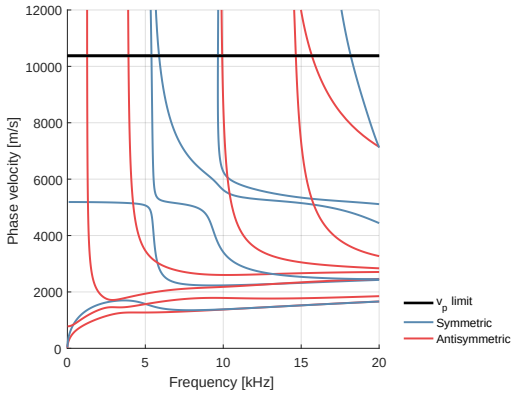

(c) Phase velocity-Frequency curves.

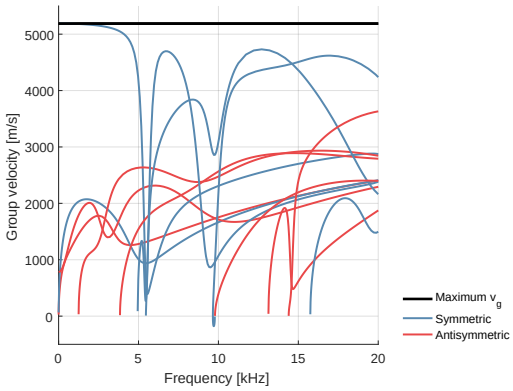

(d) Group velocity-Frequency curves.

Figure 4: SAFE mesh with piezoelectric transducer attached and associated dispersion curves for UIC60 rail.

If $p > m$, the over-defined system of equations is solved in a least-squares sense using the Moore-Penrose generalised inverse (also called the pseudo inverse). The matrix $\bar{\mathbf{\Psi}}$ should have rank m if there are at least m different propagating modes at the frequency of interest.

The results in Section 5 are generated using displacement signals extracted from 200 randomly distributed nodes between 0.5m and 1m from the centre of the transducer as illustrated in Figure 2.

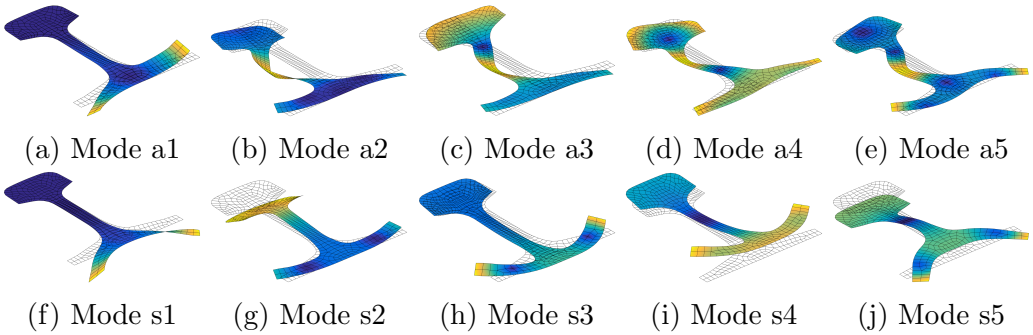

(a) Mode a1 (b) Mode a2 (c) Mode a3 (d) Mode a4 (e) Mode a5

(f) Mode s1 (g) Mode s2 (h) Mode s3 (i) Mode s4 (j) Mode s5

Figure 5: Antisymmetric modes a1 to a5 and symmetric modes s1 to s5 computed at 10 kHz.

5. Results

This section presents the results of the numerical comparison between Abaqus/Explicit and SAFE-3D. The problem under consideration is illustrated in Figure 2, and is depicted for the SAFE-3D case in Figure 4a. Figures 4b to 4d depict the dispersion curves for the UIC60 rail with material properties as given in Figure 2. Modes are separated exploiting the fact that for a symmetric waveguide, families of symmetric and antisymmetric modes can cross, but the dispersion curves within a symmetric or antisymmetic family approach and then repel each other and do not cross [31].

Figure 5 shows the mode shapes of all the propagating modes at 10kHz. The mode numbering scheme proposed in [31] is used to number the modes with an 'a' or 's' to represent antisymmetric and symmetric modes, respectively followed by a number representing the order in which cut-off occurs on the frequency axis. So, for example the 3rd symmetric mode to cut-off is numbered s3.

In order to study the effects of cut-off, a frequency range with an isolated cut-off frequency is required. To this end a convenient frequency range was found to be around 10kHz. The two modes which cut-off close to 10kHz are antisymmetric mode a5 and symmetric mode s5. Given the mode shapes however, it was noted that a transducer attached to the web of the rail preferentially excites the antisymmetric modes, and generally the symmetric modes have a small influence on the overall response. Frequencies around 7kHz do not have any cut-offs, and this frequency was therefore chosen to compare results with, so that the effects at cut-off can be isolated.

5.1. Compliance comparison

In order to verify the receptance computed using the procedure described in Section 2.4.3, a comparison with Abaqus/Explicit is performed. A force is applied at the location corresponding to the centre of the transducer front mass, denoted Node 1 in Figure 4a, and the displacement computed at two different locations, namely Node 1 and Node 2 highlighted in the same figure.

A 10.5 cycle Hanning windowed toneburst (with 7kHz and 10kHz centre frequency, respectively) point force is applied in the $x-$direction. Both the displacement response and the force are converted to the frequency domain and frequency response in terms of both amplitude and angle determined. The same information is extracted from the SAFE-3D interaction as computed in the receptance matrix $\boldsymbol{R}_w$ in (36). The results are plotted for displacements in the $x-, y-$ and $z-$directions in Figure 6. The plots reflect only frequencies where the amplitude of the Fourier Transform of the forcing function is above 1% of the maximum amplitude. As a result, the accuracy at the upper and lower frequency limits are not expected to be as good as those at the centre of the frequency range.

Figures 6a and 6b depict the amplitude and angle of the receptance for a 7kHz centre frequency toneburst applied at Node 1 and measured at the same node. There is a slight amplitude difference between the SAFE-3D results and the Abaqus/Explicit results. This is possibly attributed to discretisation of the Abaqus/Explicit model in the $z-$direction, effectively distributing the force over two element lengths in the $z-$direction, whereas the SAFE-3D model treats the $z-$direction analytically. Furthermore, responses close or at the point of excitation consist of contributions from many evanescent modes which quickly decay in the propagation direction. The displacement in the $x-$direction naturally dominate the response, since the force is applied in that direction. The $z-$component of displacement is very small (or zero) due to symmetry, which is the reason the the random angle of the frequency response. On the whole, excellent agreement is achieved between the two models.

Figures 6c and 6d show the response, again for the 7kHz excitation but with the response computed in this case at Node 2, where the $z-$displacements have developed. The response is relatively regular again, due to the fact that there are no modes with cut-offs excited in the frequency range considered. Once again, good agreement between the Abaqus/Explicit and the SAFE-3D results are achieved, although in this case the Abaqus/Explicit amplitudes are generally slightly smaller than the SAFE-3D results. It is remarkable

that, although Node 2 is only 7.5 mm away from the source, displacements are four times smaller at Node 2 than at the source.

Figures 6e and 6f present the frequency response with the 10kHz centre frequency toneburst applied. In this case, the a5 mode cuts off in the frequency range considered, and is strongly excited by the force applied to the web. Although the s5 mode also cuts on in this frequency range, it was found that the response of symmetric modes due to the chosen excitation is small. The peak in the frequency response function corresponds to the resonance-like behaviour that is expected when driving a mode close the its cut-off frequency. The two models predict slightly different cut-off frequencies, with the Abaqus/Explicit results being at a slightly lower frequency than the SAFE-3D prediction. Apart from the slight frequency shift, the two models have very similar behaviour at frequencies with relatively high energy content (9-11 kHz). It should be noted that, without a SAFE analysis it would not have been obvious that this behaviour is as a result of a mode cut-off.

5.2. Time domain comparison

In this section, the time domain results will be compared for the problem illustrated in Figure 2. Since the response is dominated by the displacement in the $x-$direction, only u_x displacements are presented at a distance of 1 m from the transducer centroid, at the same point on the cross-section as the transducer centroid. The piezoelectric transducer is driven using a 1 V 10.5 cycle Hanning windowed toneburst across the 4.3mm height of the piezoelectric material. Centre frequencies of 7kHz and 10kHz are considered with various strategies used to eliminate numerical issues at cut-off when using the SAFE-3D method.

Figures 8a and 8b depict the u_x response for the 7kHz case, which is used to demonstrate that nodes are not required to be coincident for the proposed method. The case where the SAFE and transducer nodes are not coincident is depicted in Figure 7, and will be denoted SAFE-3D* in the results. Good agreement between the Abaqus/Explicit and SAFE-3D results is achieved without any need to alleviate the effects of ringing since no cut-off is excited in this case. The two sets of SAFE results are almost identical. It is not clear if the small difference between the two SAFE results is as a result of the transducer mesh distortion or the interpolation scheme to transfer forces and displacements. The fact that nodes are not required to be coincident is

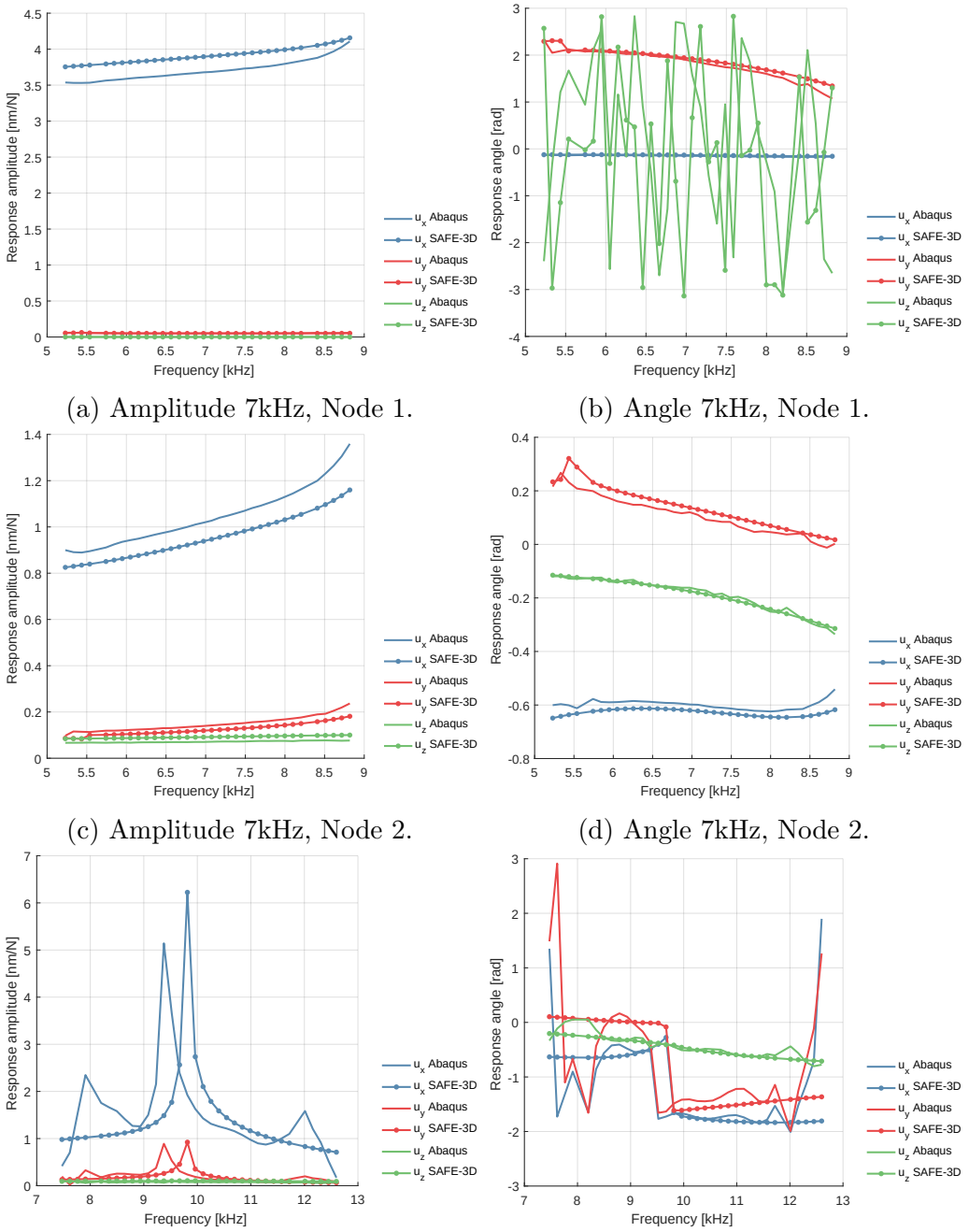

(a) Amplitude 7kHz, Node 1.

(b) Angle 7kHz, Node 1.

(c) Amplitude 7kHz, Node 2.

(d) Angle 7kHz, Node 2.

(e) Amplitude 10kHz, Node 2.

(f) Angle 10kHz, Node 2.

Figure 6: Compliance comparison - Abaqus/Explicit and SAFE-3D.

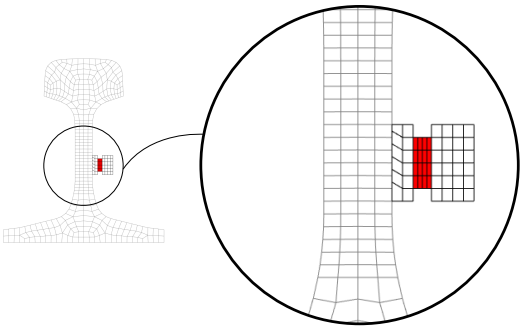

Figure 7: Illustration of distorted mesh for the case where nodes are not coincident.

further demonstrated in [8], where the SAFE-3D method was used to design an optimal transducer without presenting the analysis method itself.

Figure 8c and 8d show the response due to the 10 kHz excitation. In Figure 8c, the Abaqus/Explicit response is presented together with the post-processing based methods to eliminate the ringing associated with exciting a mode close to a cut-off frequency. The results without any scheme to treat the effects of cut-off are denoted SAFE-3D in the figure, and in this case it is difficult to determine the first arrival due to the wrap-around effect. The results with causality enforced as detailed in Section 3 are denoted SAFE-3D-C and show a vast improvement over the response with no intervention. Results produced by filtering responses with high phase velocity as explained in Section 3 are labelled SAFE-3D-V and produced similar results to the case where causality is enforced, except that a slight wrap-around effect is still present making it difficult to determine the first arrival. A combination of limiting the response based on phase velocity and causality could also be implemented, but these results are not shown for brevity. The phase difference between the Abaqus/Explicit results and the SAFE-3D results after approximately 1.5 ms is thought to be due to the difference in cut-off frequency for mode a5 (and associated ringing behaviour) noted in Figures 6e and 6f.

Figure 8d depicts the results with damping added, instead of using post-processing techniques. Three different damping levels are evaluated as explained in Section 3, i.e. the values proposed by Bartoli *et al.* [19] denoted '$1.0 \times (\kappa_L, \kappa_T)$' as well as values 10 times higher '$10 \times (\kappa_L, \kappa_T)$' and ten times smaller '$0.1 \times (\kappa_L, \kappa_T)$'. The results confirm that the material properties suggested in [19] effectively damp the unrealistically large displacements and

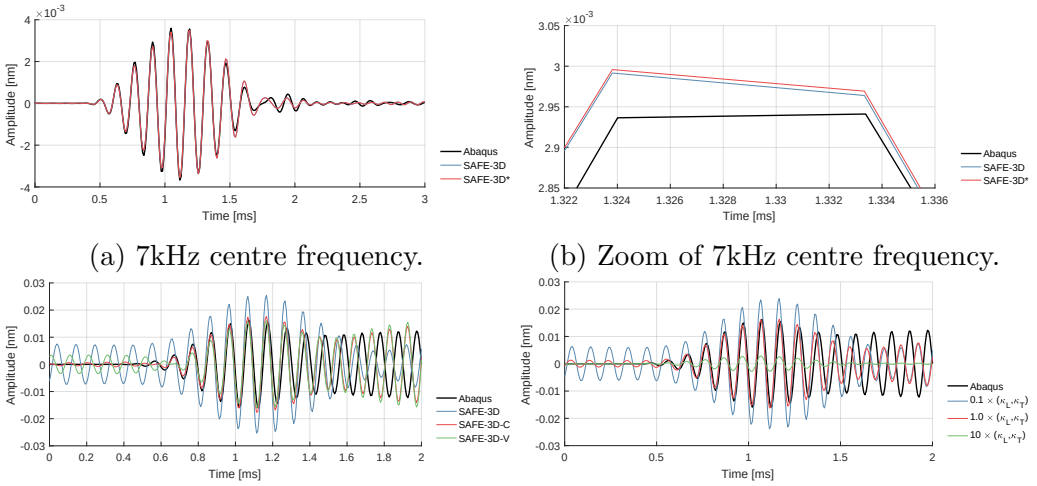

(a) 7kHz centre frequency.

(b) Zoom of 7kHz centre frequency.

(c) 10kHz centre frequency, causality and velocity filtering.

(d) 10kHz centre frequency, damped results.

Figure 8: Displacement u_x at $z = 1$m.

very good agreement with the Abaqus/Explicit results are achieved. The lower damping values produce results very similar to those where no damping is included, whereas it is clear that over damping the response results in an underestimation of the response. The important point is, however, that for each damping parameter tested the dispersion curves and the modal amplitudes need to be re-calculated and since damping is usually 'tuned' to match experimental measurements, this could be numerically expensive and requires good, quantitative experimental results. On the other hand, post-processing methods such as those evaluated in Figure 8c, can be tuned without having to recompute dispersion curves or modal amplitudes.

5.3. Frequency domain comparison

Time traces of displacement are useful when comparing simulation and experimental results. Displacement signals on their own are, however, not necessarily a very rich source of information. Instead, what is required for transducer design is information about how well a certain (targeted) propagating mode is excited. Targeted modes would typically have energy concentrated in the region of the waveguide where discontinuities are sought, and be as non-dispersive as possible [8]. To this end, it is advantageous to present the results in the frequency domain as modal amplitudes.

The SAFE-3D method computes modal amplitudes for each individual mode at different frequencies naturally. The accuracy of modal amplitudes close to cut-offs have not previously been investigated using SAFE-3D, and instead frequencies containing cut-offs have simply been avoided [8]. Here a quantitative comparison between SAFE-3D and Abaqus/Explicit is performed. The problem described in Section 5.2 and Figure 2 is considered again with the same voltage excitation as in Section 5.2. Since only the antisymmetric modes are strongly excited from this transducer location, only these modes are presented in Figure 9.

Figure 9a depicts modal amplitudes computed using SAFE-3D, and those extracted from Abaqus/Explicit results using the process presented in Section 4.3 for 7kHz centre frequency case. Excellent agreement is achieved between the modes extracted from the Abaqus/Explicit results and those computed using the SAFE-3D method. Although the excitation has a 7kHz centre frequency, not all of the antisymmetric modes presented have a maximum at 7kHz. This is possibly due to the mode shapes (and the associated modal amplitudes) being frequency dependent.

Results for the 10kHz centre frequency excitation are presented in Figure 9b. In this case, an additional mode (a5) is seen to cut-off on the frequency axis between 9 and 10 kHz. Considering first the SAFE-3D results, the modal amplitude of mode a2 rises as the cut-off frequency of mode a5 is approached. As the cut-off frequency is reached, a discrete drop in the modal amplitude of a2 is observed as energy is used to excite mode a5.

It was noted from Figures 6e and 6f that the cut-off frequency for the Abaqus/Explicit model is predicted at a slightly lower frequency than the SAFE-3D model. This accounts for the difference in predicted modal amplitudes between the cut-off frequencies predicted using the two models, where essentially the incorrect basis functions (SAFE eigenvectors) are used to extract modes from the Abaqus/Explicit results. Despite these discrepancies similar trends are observed between the two sets of results, even close to the cut-off frequency. For example, in both cases mode a2 has the highest modal amplitude, followed by modes a5 and then a3. This information would be useful for transducer design. At frequencies away from the cut-off frequency (below 9kHz and above 11kHz) better agreement is achieved.

In order to improve the agreement, either mesh refinement strategies could be employed in both the SAFE-3D, but especially in the Abaqus/Explicit model, or the SAFE model could be modified (in terms or material properties or small geometrical modifications) in order to achieve a better agreement in

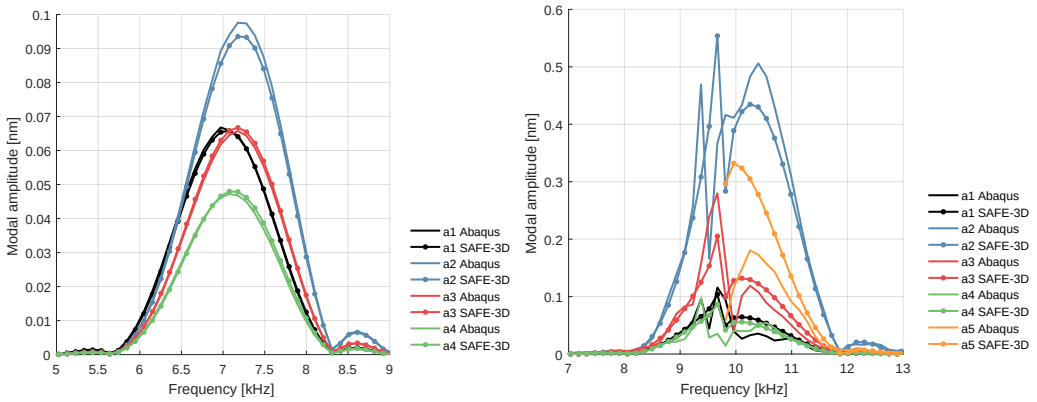

(a) 7kHz centre frequency. (b) 10kHz centre frequency.

Figure 9: Modal amplitudes extracted from Abaqus/Explicit and computed using SAFE-3D.

the predicted cut-off frequencies between Abaqus/Explicit and SAFE-3D.

6. Conclusions

A method to efficiently couple a conventional 3D finite element (FE) model of a piezoelectric transducer to a 2D semi-analytical finite element (SAFE) model of a waveguide is presented. The method is referred to as SAFE-3D. The proposed procedure is efficient for transducer design since various transducer geometries and attachment locations can be evaluated without having to recompute the SAFE eigenvalue problem, and without requiring the SAFE and 3D FE nodes to be coincident. A numerical verification of the proposed method is presented through a comparison with results from a commercial finite element solver, Abaqus/Explicit in this case.

The SAFE-3D analysis requires an estimate of the waveguide dynamic stiffness. It is shown that the SAFE forced response accurately predicts the waveguide dynamic stiffness, even at frequencies where mode cut-offs occur. It is demonstrated, however that the SAFE-3D and Abaqus/Explicit models predict slightly different cut-off frequencies.

A time domain comparison between SAFE-3D and Abaqus/Explicit simulations of a waveguide excited by a piezoelectric transducer is performed. A thermal equivalent Abaqus/Explicit transducer model is used with absorbing boundary conditions to model the piezoelectric transducer excitation. Firstly, it is demonstrated that the SAFE-3D method does not require 3D

FE and SAFE nodes to be coincident. Next, various methods to deal with the large time domain responses predicted using the SAFE-3D method, when a mode is excited close to its cut-off frequency, are evaluated. It is shown that introducing hysteretic damping effectively reduces the response if an appropriate level of damping is introduced. However since realistic damping properties are not always known, some iteration may be required, which could be numerically expensive. Alternatively, post-processing methods were shown to have similar performance and are less numerically expensive.

Frequency domain modal amplitudes are extracted from Abaqus/Explicit time domain results using a SAFE-based method, and compared with modal amplitudes computed using SAFE-3D. Excellent agreement is achieved at frequencies where no mode cut-offs occur. However, since the Abaqus/Explicit and SAFE-3D models predict slightly different cut-off frequencies, mode extraction from Abaqus/Explicit is not as accurate close to cut-off frequencies. Despite these differences, there is acceptable agreement between the two methods, demonstrating the accuracy of the SAFE-3D method.

[1] C. Willberg, S. Duczek, J. M. Vivar-Perez, Z. A. B. Ahmad, Simulation methods for guided wave-based structural health monitoring: A review, Applied Mechanics Reviews 67 (2015) 010803.

[2] P. Loveday, D. Ramatlo, F. Burger, Monitoring of rail track using guided wave ultrasound, in: Proceedings of the 19th World Conference on Non Destructive Testing (WCNDT 2016), Munich, Germany, 2016, pp. 3341–3348.

[3] L. Gavrić, Computation of propagative waves in free rail using a finite element technique, Journal of Sound and Vibration 185 (3) (1995) 531–543.

[4] T. Hayashi, W.-J. Song, J. Rose, Guided wave dispersion curves for a bar with an arbitrary cross-section, a rod and rail example, Ultrasonics 41 (2003) 175–183.

[5] V. Damljanović, R. Weaver, Forced response of a cylindrical waveguide with simulation of the wavenumber extraction problem, The Journal of the Acoustical Society of America 115 (4) (2004) 1582–1591.

[6] P. Loveday, Analysis of piezoelectric ultrasonic transducers attached to waveguides using waveguide finite elements, IEEE Transactions on Ultrasonics, Ferroelectrics and Frequency Control 54 (10) (2007) 2045 – 2051.

[7] P. Loveday, Simulation of piezoelectric excitation of guided waves using waveguide finite elements, IEEE Transactions on Ultrasonics, Ferroelectrics and Frequency Control 55 (9) (2008) 2038 – 2045.

[8] D. Ramatlo, D. Wilke, P. Loveday, Development of an optimal piezoelectric transducer to excite guided waves in a rail web, submitted to NDT & E International.

[9] P. Lowe, S. Fateri, R. Sanderson, N. Boulgouris, Finite element modelling of the interaction of ultrasonic guided waves with coupled piezoelectric transducers, Insight - Non-Destructive Testing and Condition Monitoring 56 (9) (2014) 505–509.

[10] S. Fateri, P. Lowe, B. Engineer, N. Boulgouris, Investigation of ultrasonic guided waves interacting with piezoelectric transducers, IEEE Sensors Journal 15 (8) (2015) 4319–4328.

[11] M. Kalkowski, E. Rustighi, T. Waters, Modelling piezoelectric excitation in waveguides using the semi-analytical finite element method, Computers and Structures 173 (2016) 174–186.

[12] K. Jezzine, A. Lhémery, Diffraction effects on ultrasonic guided waves radiated or received by transducers mounted on the section of the guide, in: AIP Conference Proceedings, Vol. 820, 2006, pp. 134–141.

[13] H. Taweel, S. Dong, M. Kazic, Wave reflection from the free end of a cylinder with an arbitrary cross-section, International Journal of Solids and Structures 37 (2000) 1701–1726.

[14] H. Allik, T. Hughes, Finite element method for piezoelectric vibration, International Journal for Numerical Methods in Engineering 2 (1970) 151–157.

[15] F. Treysséde, L. Laguerre, Numerical and analytical calculation of modal excitability for elastic wave generation in lossy waveguides, Journal of the Acoustical Society of America, Acoustical Society of America 133 (2013) 3827–3837.

[16] V. Damljanović, R. Weaver, Propagating and evanescent elastic waves in cylindrical waveguides of arbitrary cross section, The Journal of the Acoustical Society of America 115 (4) (2004) 1572–1581.

[17] F. Treysséde, Elastic waves in helical waveguides, Wave Motion 45 (2008) 457–470.

[18] A. Bernard, M. J. S. Lowe, M. Deschamps, Guided waves energy velocity in absorbing and non-absorbing plates, The Journal of the Acoustical Society of America 110 (1) (2001) 186–196.

[19] I. Bartoli, A. Marzani, F. Lanza di Scalea, E. Viola, Modeling wave propagation in damped waveguides of arbitrary cross-section, Journal of Sound and Vibration 295 (2006) 685–707.

[20] D. K. Stoyko, Using the Singularity Frequencies of Guided Waves to Obtain a Pipe's Properties and Detect and Size Notches, Ph.D. thesis, The University of Manitoba, Winnipeg, Manitoba, Canada (2012).

[21] A. Marzani, Time-transient response for ultrasonic guided waves propagating in damped cylinders, International Journal of Solids and Structures 45 (2008) 6347–6368.

[22] O. Mukdadi, S. Datta, Transient ultrasonic guided waves in layered plates with rectangular cross section, Journal of Applied Physics 93 (11) (2003) 9360–9370.

[23] P. Rajagopal, M. Drozdz, E. Skelton, M. Lowe, R. Craster, On the use of absorbing layers to simulate the propagation of elastic waves in unbounded isotropic media using commercially available Finite Element packages, NDT & E International 51 (2012) 30–40.

[24] J. Pettit, A. Walker, P. Cawley, M. Lowe, A Stiffness Reduction Method for efficient absorption of waves at boundaries for use in commercial Finite Element codes, Ultrasonics 54 (2014) 1868–1879.

[25] J. Harley, J. Moura, Sparse recovery of the multimodal and dispersive characteristics of Lamb waves, The Journal of the Acoustical Society of America 133 (5) (2013) 2732–2745.

[26] M. Zhao, L. Zeng, J. Lin, W. Wu, Mode identification and extraction of broadband ultrasonic guided waves, Measurement Science and Technology 25 (2014) 115005.

[27] W. Duan, R. Kirby, A numerical model for the scattering of elastic waves from a non-axisymmetric defect in a pipe, Finite Elements in Analysis and Design 100 (2015) 28–40.

[28] B. Pavlakovic, D. Alleyne, M. Lowe, P. Cawley, Simulation of Lamb wave propagation using pure mode excitation, in: Review of Progress in Quantitative Nondestructive Evaluation, 1998, pp. 1003–1010.

[29] P. Loveday, Measurement of modal amplitudes of guided waves in rails, Proceedings of SPIE 6935 (2008) 69351J.

[30] P. Loveday, C. Long, Laser vibrometer measurement of guided wave modes in rail track, Ultrasonics 57 (2015) 209–217.

[31] P. Loveday, C. Long, D. Ramatlo, Mode repulsion of ultrasonic guided waves in rails, Ultrasonics 84 (2018) 341–349.

Acknowledgements

The first author would like to thank Dr. D.K. Stoyko for his valuable insights regarding the enforcement of causality.